

COMBINED TOPOLOGY AND COMPOSITE LAMINATE OPTIMIZATION OF A STRUT-BRACED DRY WING FOR A HYDROGEN AIRCRAFT

Lander Vertonghen[1], Charly Mollet[2], Cédric Julien[1] & François-Xavier Irisarri[1]

[1]DMAS, ONERA, Université Paris-Saclay, 92320, Châtillon, France
[2]DAAA, ONERA, Institut Polytechnique de Paris, 92320, Châtillon, France

Abstract

This paper presents the advanced and innovative design of a LH2-powered Strut-Braced Wing (SBW), issued from an overall aircraft design optimization process. A bi-level optimization framework is first applied to the composite design of a conventional wingbox concept with ribs and stiffeners. The approach begins with a homogenized stiffness optimization aimed at mass minimization under strength and buckling constraints, followed by a discrete laminate retrieval step. To further investigate the structural potential and expanded design space enabled by a Strut-Braced Dry Wing (SBDW) configuration, an extended optimization strategy is introduced. This method couples topology optimization of both the wing and strut cores with bi-level composite layup optimization of the skins and spars.

Keywords: MDO, LH2-powered aircraft, lamination parameters, bi-level optimization

1. General Introduction

In the context of reducing the environment impact of aviation, the conventional kerosene powered cantilever wing aircrafts seem close to their performance limits. An ever quest for better fuel efficiency and near zero CO_2 emissions prompts the search for new architectures that combine innovative layouts with alternative energy. Very high aspect ratio wings are identified as promising to increase the overall aircraft efficiency, coupled to liquid hydrogen (LH2) propulsion. Furthermore, in this type of configuration, LH2 tanks are stored inside the fuselage for such configurations. This frees the wing from any fuel volume constraints and enables new possibilities for a dry wing design. This freedom allows designers to create wings with novel internal load-bearing structure. Moreover, to take advantage of the aerodynamic benefits of a very high aspect ratio and thin wings without incurring prohibitive structural weight, a supporting strut is added, leading to a favorable aero-structural compromise. Within the Clean Aviation UP Wing project, ONERA, TU Delft and the University of Stuttgart are studying such an LH2 Strut-Braced Wing (SBW) concept (2500 Nm, 239 passengers, Mach 0.78) aiming at minimizing in-flight energy consumption by performing a multidisciplinary optimization [1].

This paper focuses on the advanced structural design of a fixed aircraft configuration obtained as the optimal solution from a multidisciplinary design optimization process. The study first investigates the composite optimization of a conventional wing structure featuring ribs and stiffeners under critical loadcases. The optimization variables include the stiffener cross-sections as well as the laminate layups of the composite skins, spars, and ribs. Subsequently, a dry-wing structural concept is explored by replacing the conventional rib-and-stiffener architecture with a more flexible structural core design. Extended design space is achieved through the topology optimization of the wingbox and strutbox core structures using an isotropic material, coupled with the composite optimization of the encompassing load-carrying surfaces. This approach enables the assessment of possible novel and innovative structural tendencies.

This paper is setup as follows: Section 2. presents the structural model of the current best aircraft configuration, with a conventional rib and stiffener modeling concept. Section 3. details the methodology used to perform a composite optimization on this conventional configuration. Section 4. is about the methodology and parametrization to replace the ribs and stiffeners by topology optimization. Finally, Section 5. showcases results of both the conventional and dry-wing concepts for a strut-braced wing, with conclusions and outlook discussed in Section 6..

2. Aircraft Configuration

A Multidisciplinary Design Analysis and Optimization (MDAO) process with a Design of Experiment (DoE) approach has been used to obtain the best overall aircraft parameters for the design mission, as discussed in more detail by Stragiotti *et al.* [2]. For more information on the aerodynamic and structural evaluations of the DoE configurations, see Losada Costoso *et al.* [3] and Mollet *et al.* [4] respectively. Table 1 summarizes the main properties and relevant characteristics of the optimal structural configuration.

Table 1 – Properties of the optimized aircraft configuration.

MTOW	94.6 [t]	Strut/wing sweep ratio	0.658 [-]
Aspect Ratio	22.91 [-]	LAF	0.28 [-]
Strut span ratio	0.48 [-]	LAF span ratio	0.6 [-]

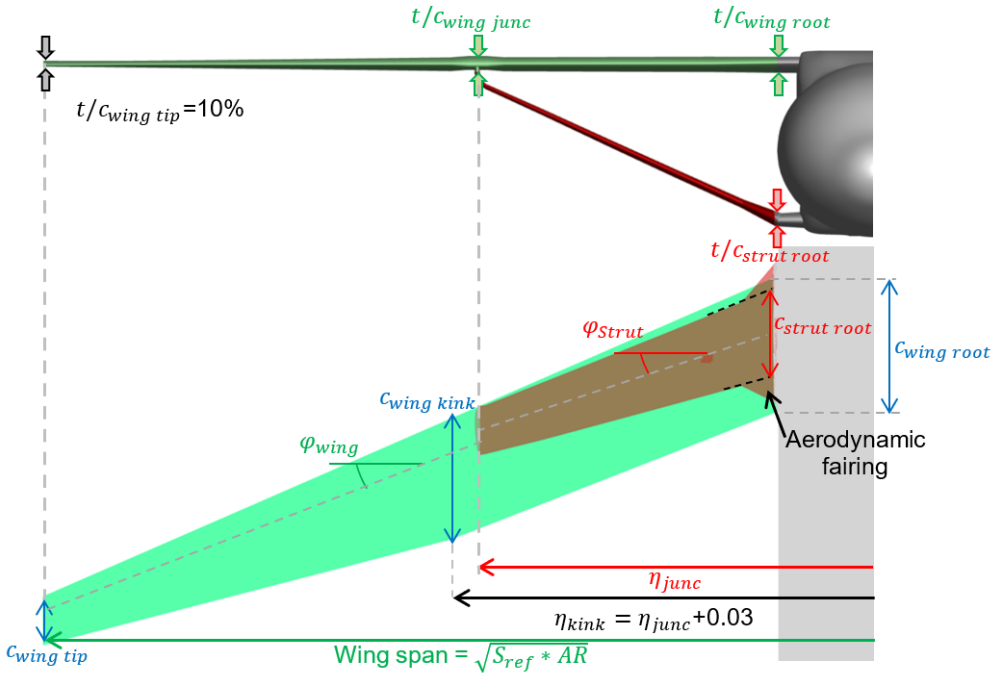


Figure 1 – Parametrization of the SBW configuration.

2.1 Load Cases

The DoE and current structural optimizations are performed using three designing load cases: a 2.5 g Manoeuvre Load Alleviation (MLA) load case, and an elliptic $\pm$ 1 g load case. The MLA load case accounts for the effect of load alleviation systems on the lift distribution, particularly to reduce loading towards the wingtip. It is a modified elliptic lift distribution, parametrized by only a Load Alleviation Factor (LAF), as the spanwize breakpoint is fixed. The LAF dictates the swing in lift from the outboard wing part, to the inboard region. A higher LAF implies that the load is reduced in the wing tip region and, consequently, increased near the wing root, as illustrated in Figure 2. The drop in lift distribution

in the center part simulates the decrease in lift due to the fuselage. Furthermore, the strut is considered non-lifting from the structural point of view. A safety factor of 1.5 is applied to all load cases.

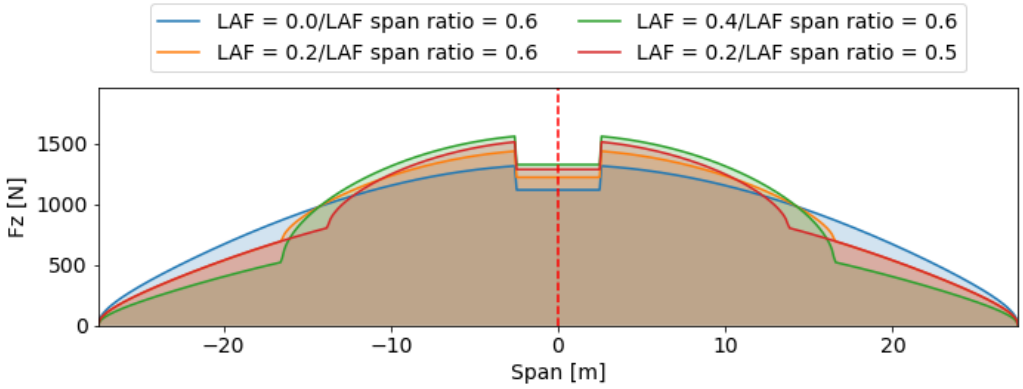


Figure 2 – MLA lift distribution for varying LAF and LAF span ratio values.

2.2 Structural Model

The structural optimizations are performed on a fixed aircraft configuration, displayed in Figure 3, consisting in a wingbox design with the skin, spars and ribs as shell elements and the stiffeners as beam elements. The strut is composed similarly to the wing, but without stiffeners, as the strutbox dimensions are insufficient to accommodate them. The strut connection to the wing and fuselage is assumed to be rigid and therefore represented by a clamped condition at both ends. This also reduces the effective length for Euler buckling of the strut.

The color of the element sets in Figure 3 represent zones sharing the same properties for which a different set of design variables is assigned. For each bay (i.e., the space between two consecutive ribs), separate design variables are used for the ribs, the upper and lower skins, as well as for the front and rear spar. Each distinct zone has a thickness and a set of composite variables. Finally, for the wingbox only, stiffeners are present for each bay. A distinction is made between the top and bottom stiffeners, and the top and bottom sparcaps, each with their respective design variables.

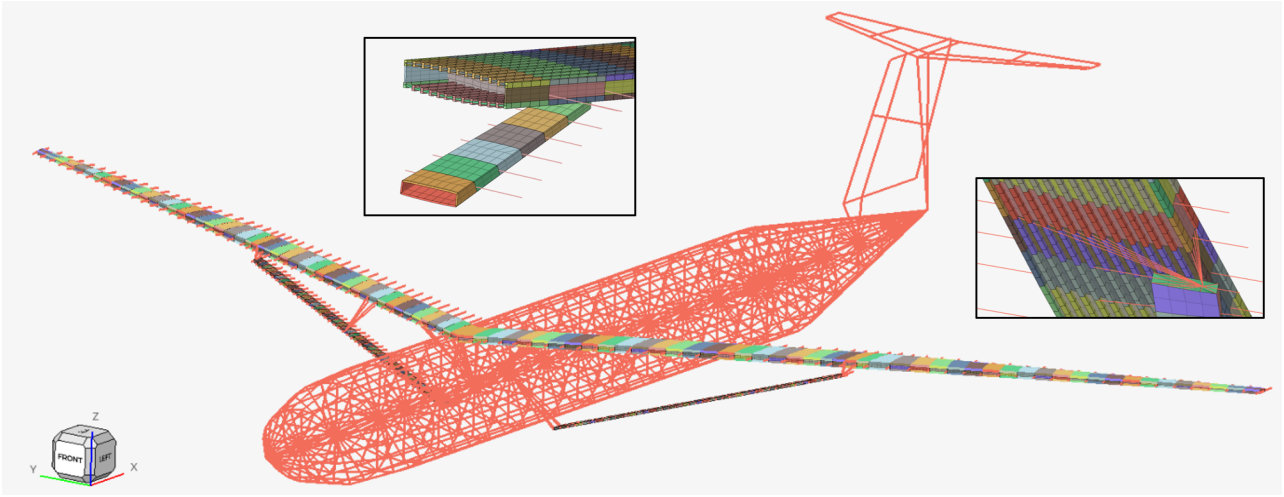


Figure 3 – Conventional wingbox structural model and mesh.

Figure 4 shows the discretized model loads from a MLA load case. These forces are introduced at the quarter chord of each rib. The drop in model loads around the strut junction is solely related to the discretization of the lift over a a tigther spaced ribs at the junction.

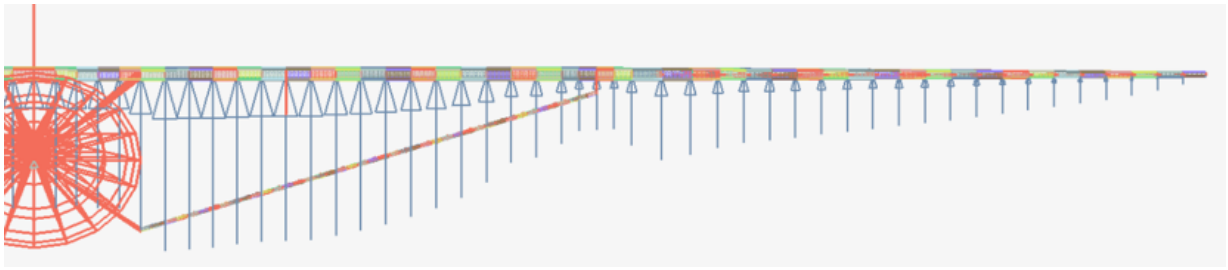


Figure 4 – Discretized loads for the 2.5 g MLA condition on the conventional structural model.

2.3 Material Properties

All structural optimizations are performed using the properties of the M21/IMA-12K Uni-Directional (UD) ply. It is used as base ply for the composite laminate optimization, and for equivalent isotropic properties for the topology optimization part. The material properties of the UD ply are listed in Table 2.

Table 2 – Base ply UD material properties.

E_{11} [GPa]	E_{22} [GPa]	G_{12} [GPa]	ν_{12} [-]	Tensile ε [-]	Compressive ε [-]	h_{ply} [mm]
149.0	10.0	5.2	0.302	10e-6	-3.5e-6	0.184

Equivalent isotropic stiffness properties (called *black aluminum*) are also derived from this base ply. The *black aluminum* properties are obtained from the isotropic part of the UD ply of Table 2. This is equivalent to the E and ν of a Quasi-Isotropic layup. The yield stress σ^Y for the *black aluminum* is obtained as the stress limit of the lowest magnitude of th UD ply strain allowable ε times the *black aluminum* Young's modulus.

Table 3 – Equivalent *black aluminum* isotropic material properties.

E [GPa]	G [GPa]	ν [GPa]	σ^Y [MPa]
57.24	21.84	0.31	200.0

3. Composite Wing Design Methodology

To optimize the composite layout, a bi-level optimization strategy is used. Initially, an optimization of the homogenized stiffness is performed using continuous thickness. Afterwards, a stacking sequence retrieval is performed considering the discrete thickness and layups of the laminates to match as closely as possible the stiffness distribution obtained with the first level optimization.

Both optimization levels are based on the same composite mechanical behavior, represented by means of the Classical Laminate Plate Theory (CLPT). This links the membrane (N) and bending moments (M) to the in-plane strains (ε_0) and curvatures (κ) through the ABD matrix as follows:

$$\begin{bmatrix} N \\ M \end{bmatrix} = \begin{bmatrix} A & B \\ B & D \end{bmatrix} \begin{bmatrix} \varepsilon_0 \\ \kappa \end{bmatrix} \tag{1}$$

For the composite layup, the assumptions of balanced and symmetric laminate (to avoid the unwanted in-plane/out-of-plane coupling behavior represented by B), and an orthotropic behavior in D are enforced.

3.1 Homogenized Stiffness Optimization

3.2 Parametrization

The homogenized composite properties of the first step are represented by a continuous thickness, t, and by means of the lamination parameters (LP) [5]. With the aforementioned layup assumptions, only 4 LP remain: V_A^1,V_A^3,V_D^1,V_D^3. The LP are then defined as:

$$V_{A,D}^1, V_{A,D}^3 = \frac{1}{N}\sum_{k=1}^{N}\cos(2\theta_k, 4\theta_k)\,. \tag{2}$$

These 4 LP represent the layup information, containing both the number of equal thickness plies N and their orientation θ, as shown in Equation 2. To obtain the ABD matrix, the LP are combined with material properties of the base ply (represented here by the matrices $\Gamma_{0,1,3}$), as expressed in Equation 3:

$$\begin{aligned}[A] &= t(\Gamma_0 + \Gamma_1 V_A^1 + \Gamma_3 V_A^3)\\ [D] &= \frac{t^3}{12}(\Gamma_0 + \Gamma_1 V_D^1 + \Gamma_3 V_D^3)\end{aligned} \tag{3}$$

Γ are matrices with material properties expressed by means of the Tsai-Paganao parameters defined in a fixed reference frame, with respect to the components of the base ply properties [6].

During the optimization, the LP are design variables that represents the composite laminate. The LP values are bound by trigonometric relations, which become additional optimization constraints, according to:

$$\begin{aligned}1 + V_{A,D}^3 - 2(V_{A,D}^1)^2 &\geq 0\,,\\ V_{A,D}^3 &\leq 1\,.\end{aligned} \tag{4}$$

Finally, it is common practice to include at least 10% of 0°/±45°/90° fibers in the layup, to account for susceptible loads happening outside of the considered load case in the design. This rule is taken into account on the in-plane properties A as equivalent stiffness as follows [7], where p is the percentage of 0°/±45°/90° fibers:

$$\begin{aligned}(1-4p)^2 + (1-4p)V_A^3 - 2(V_A^1)^2 &\geq 0\,,\\ 1 - 4p - V_A^3 &\geq 0\,.\end{aligned} \tag{5}$$

A representation of the reduced design space of V_A to include p% of 0°/±45°/90° fibers in the layup is given in Figure 5.

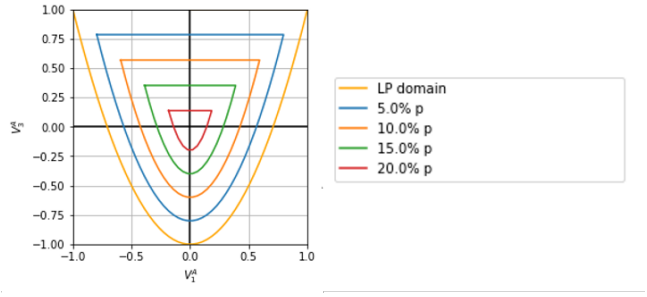


Figure 5 – V_A domain, and the reduced design space with p% of 0°/±45°/90° fibers in the layup.

3.2.1 Composite Laminate Strength

The strength constraint for the composite is defined by a maximum tensile and compressive strain along the fiber. As homogenized stiffness properties are used, and no physical stacking sequence is

available, the maximum strain criterion is applied at the outer (top and bottom) edge of the laminate, $h/2$. The strain components of ε ($\varepsilon_{xx}, \varepsilon_{yy}$ and γ_{xy}) are obtained according to:

$$\varepsilon = \varepsilon_0 \pm \frac{h}{2}\kappa, \quad \text{where} \quad \begin{bmatrix}\varepsilon_0 \\ \kappa\end{bmatrix} = \begin{bmatrix}A & B \\ B & D\end{bmatrix}^{-1} \begin{bmatrix}N \\ M\end{bmatrix}. \tag{6}$$

Both compressive and tensile strain allowables are then compared to the maximum principal strain to define the strength criterion.

3.2.2 Optimization Problem Statement

The objective of the optimization is to minimize the mass of the structure under several load cases with different mechanical constraints for each. The optimization constraints include strength and buckling considerations. Material strength is evaluated as explained in Section 3.2.1. Furthermore, buckling is evaluated by solving a linear eigenvalue problem, and should not occur for the applied loads, meaning the buckling load multiplier $\lambda_{crit} \geq 1$. The optimization problem is solved by means of a gradient-based optimization with the SQP algorithm within Optistruct [8], and reads as:

$$\min_{\{t_{stiff}\},\{t_{shell}\},\{V_A^1\},\{V_A^3\},\{V_D^1\},\{V_D^3\}} \text{mass}\left(\{t_{stiff}\},\{t_{shell}\}\right)$$
$$\text{s.t.} \begin{cases} \text{strength}(\{t_{stiff}\},\{t_{shell}\}),\{V_A^1\},\{V_A^3\},\{V_D^1\},\{V_D^3\}) \\ \text{buckling}(\{t_{stiff}\},\{t_{shell}\}),\{V_A^1\},\{V_A^3\},\{V_D^1\},\{V_D^3\}) \\ (1-4p)^2 + (1-4p)\{V_A^3\} - 2\{V_A^1\}^2 \geq 0 \\ 1-4p-\{V_A^3\} \geq 0 \\ 1+\{V_D^3\} - 2\{V_D^1\}^2 \geq 0 \\ 1-\{V_D^3\} \geq 0 \\ \{t_{shell}\},\{t_{stiff}\} \in [t_{\min}, t_{\max}] \\ \{V_{A,D}^{1,3}\} \in [-1,1] \end{cases}, \tag{7}$$

where $\{\}$ represents the vector of design variables. Considering elastic materials within the assumptions of small strains and small displacements, the mechanical response is obtained from a mechanical analysis by means of the Finite Element Method (FEM), where the displacement vector $\{U\}$ is the solution to $[K]\{U\} = \{F\}$, $[K]$ being the global stiffness matrix of the structure and $\{F\}$ the force vector.

A conventional wingbox concept is used, with ribs, spars, skins and stiffeners. The design variables are the thickness $\{t_{shell}\}$ and LP $\{V_A^1\},\{V_A^3\},\{V_D^1\},\{V_D^3\}$ per distinct property region, that represent either the wingbox and strutbox' skins, spars and ribs. A minimum skin thickness requirement is set, in such a way to be at least 4 mm on the top skin, and varying minimum thickness for the bottom skin. An minimum thickness of 8 mm is enforced from the fuselage to the engine pylon, whereas the minimum thickness between the engine pylon and the wingtip is set at 6 mm. Moreover, the bays directly connected to the engine pylon and strut-wing junction have a minimum skin thickness of 20 mm. The $\{t_{stiff}\}$ design variables represent the thickness of the stiffeners of the wingbox. t_{stiff} is used to compute the area and inertia of the T-shaped stiffener, knowing that the thickness-to-height ratio λ for these stiffeners is fixed at 5, as shown in Figure 6. For the stiffeners, a predefined layup of 70% $0°$, 20% $\pm 45°$ and 10% $90°$ is used. Only the thickness, and subsequent cross-sectional properties (area, inertia), of the stiffener are changed in the optimization. The same modeling and predefined layup is used for the stiffeners as for the sparcaps.

3.3 Discrete Layup Retrieval

The second step of fiber retrieval is performed using a Stacking Sequence Table (SST) optimization [9], applied to *stiffness matching* with steered fibers. *Stiffness matching* then consists in finding the best SST in such a way to minimize the difference in stiffness between the first level solution and the discrete layups with a SST. A SST ensures the continuity of the plies between zones of different

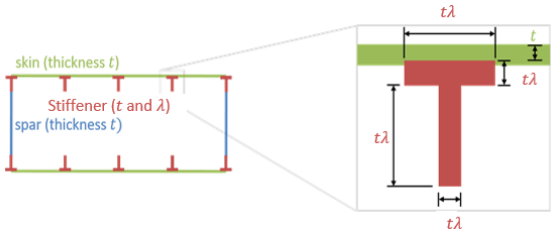


Figure 6 – Stiffener and sparcap geometry definition.

thickness, defined by a master layup sequence X_{SST}, along an insert order X_{ins} and ply number per zone X_{ply}. X_{ply} is the discrete number of plies for each region, and is obtained by rounding the first level thickness to the nearest integer multiple of the ply thickness h_{ply}. X_{SST} contains the fiber orientations for all zones and for all the ply up to the maximum thickness. Finally, X_{ins} represents the ply insertion order, where a value of 0 is assigned to all plies covering the complete domain. Consequently, the number of 0 entries in X_{ins} dictates the minimum ply count and thickness. On the other hand, the size of X_{ins} corresponds to the maximum number of plies.

In order to obtain the actual layup for a given element, the required number of plies is first determined. Orientations are then selected from the X_{SST}, starting from the layers identified by 0 in the insertion vector, and continuing to add layers in ascending order until the correct number of layers is reached. This principle is illustrated in Figure 7.

When constructing a SST, three design rules are considered, according to the assumptions of Section 3.: symmetry, balance, and the 10% rule. The symmetry and balance rules are hardcoded into the definition of the SST, whereas the 10% rule is enforced as an optimization stiffness constraint. The symmetry rule is implemented to avoid unwanted in-plane/out-of-plane coupling behavior. It is enforced by symmetrizing the relevant SST objects and by using only one half of the layup during the optimization process. The balance rule dictates that for any ply oriented at a specific angle, a corresponding ply at the opposite angle must be added to the layup. This ensures that the resulting in-plane stiffness matrix remains orthotropic.

X_{SST}	X_{ins}		X_{ply}	N = 5	N = 4	N = 3	N = 2
-45	1			-45	-45	-45	
45	3			45			
90	0	⇨		90	90	90	90
90	2			90	90		
0	0			0	90	0	0

Figure 7 – SST representation and resulting actual layups.

3.3.1 Optimization Problem Statement

The *stiffness matching* optimization problem reads as:

$$\begin{aligned} \min_{\{X_{ply}\},\{X_{SST}\},\{X_{ins}\}} \quad & F_{ABD}(\{X_{ply}\},\{X_{SST}\},\{X_{ins}\}) \\ \text{s.t.} \quad & (1-4p)^2+(1-4p)\{V_A^3\}-2\{V_A^1\}^2 \geq 0 \quad , \end{aligned} \tag{8}$$

where the objective is computed as:

$$F_{ABD}(\theta,L_T) = tr(L(\theta)L_T^{-1})+tr(L^{-1}(\theta)L_T)-12 \quad \text{with} \quad L=\begin{bmatrix} A & B \\ B & D \end{bmatrix}, \tag{9}$$

with L_T the ABD matrix of the target first level result, and $L(\theta)$ the ABD matrix of the optimized region (computed from X_{SST}, X_{ins} and X_{ply}).

The optimization constraint is the 10% 0°/±45°/90° fibers rule according to Equation 5, where the LP values of each zone is computed by means of Equation 2. The constraint value is obtained as the amount of layups constructed from the SST that do not satisfy the 10% 0°/±45°/90° fibers rule.

3.3.2 Genetic Algorithm

The optimization process of fiber retrieval is based on a Genetic Algorithm (GA), as illustrated in Figure 8. The process begins by creating an initial population P_0 that satisfies the active design generation rules, alongside an empty archive A_0. The archive serves to store the best solutions found throughout the iterations. The objective function and optimization constraints are then evaluated on the population. A ranking is subsequently performed on $\bar{P}_i$, the union of the current population P_i and the archive A_i. The ranking prioritizes all feasible solutions, which are ordered by lowest objective. Thereafter, the ranking is completed by including all infeasible solutions, ordered by ascending constraint violation values. The archive A_{i+1} is then updated by selecting the N best individuals from this ranking.

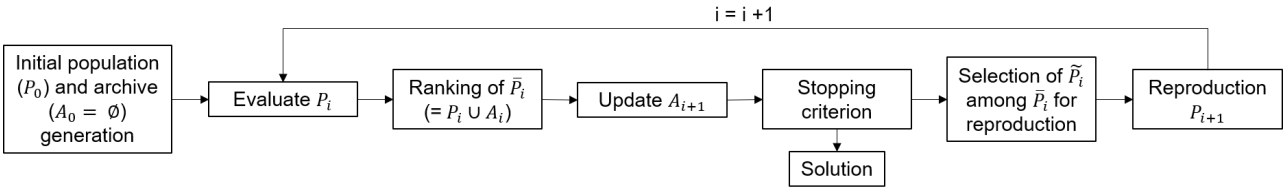


Figure 8 – Genetic algorithm flowchart for SST optimization.

A new selection for reproduction is created for the next iteration using a biased tournament with replacement. This involves drawing two random individuals from $\bar{P}_i$ and retaining one based on the following logic:

- If both individuals are feasible, the one with the lowest objective is kept.
- If only one is feasible, the feasible solution is kept.
- If both are infeasible but have identical constraint violations, the one with the lowest objective is kept. Otherwise, the individual with the lowest constraint violation is kept.

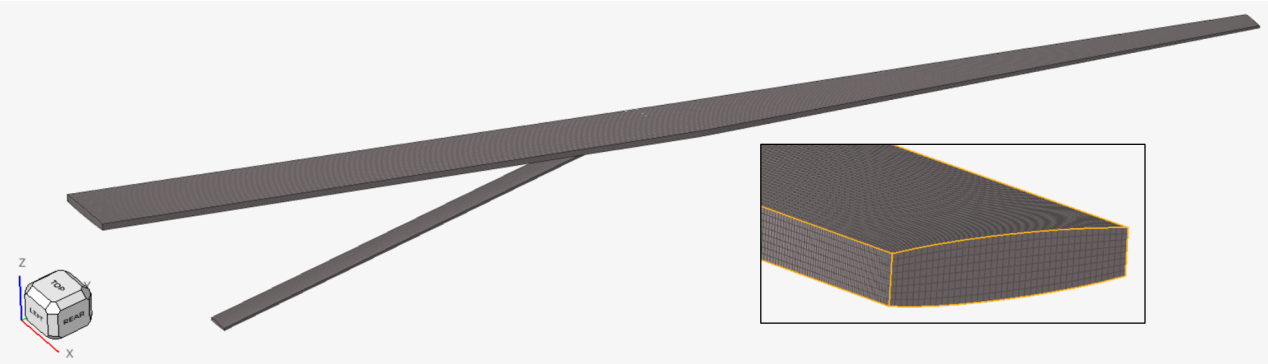
Reproduction is obtained by a probability of mutation, permutation and/or crossover operations are performed on X_{SST}, X_{ins} and X_{ply} of the selected individuals, following the methods described in [10]. Finally, the new population is evaluated again to restart the optimization loop. Convergence is enforced by a maximum number of iterations.

4. Dry Wing Design Methodology

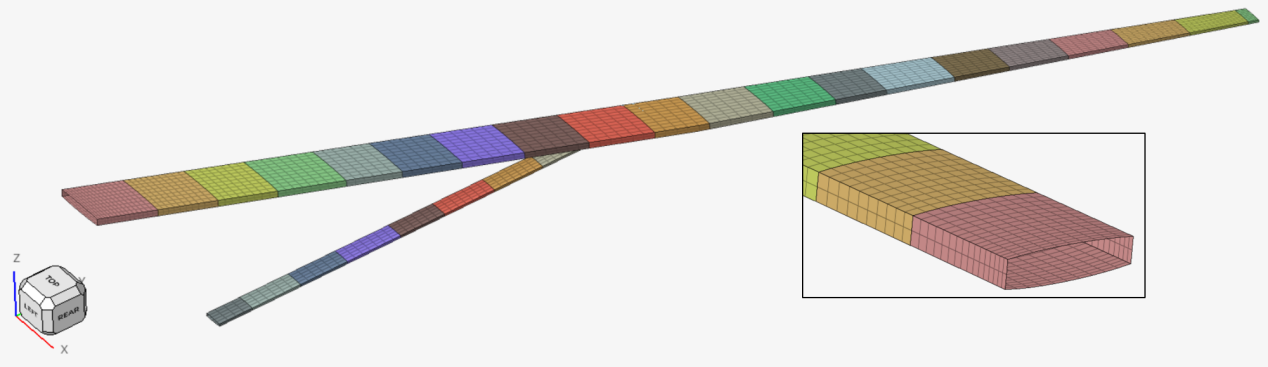
A dry wing concept is obtained by retaining the surface of the wingbox and strutbox and by removing the inner structure of a conventional wing, *i.e.* the ribs and stiffeners. They are replaced by 3D elements filling the complete core of the structure to broaden the design space, and use topology optimization in order to seek new internal material distribution. The surface of the wingbox and strutbox are still optimized with the bi-level composite optimization presented in Section 3.. The topology optimization is only used to design the core of the wing, whereas the composite optimization is still used for the surface of the wingbox and strutbox.

The model for the topology optimization is shown in Figure 9. Figure 9a is the 3D volumic mesh of the core, which is delimited at the 15% front and 65% rear chord to account for auxiliary systems

(flaps, ailerons, slats) at the leading and trailing edge. Figure 9b shows the surface mesh enclosing the 3D domain, representing the top and bottom skins as well as the front and rear spars. For the composite optimization, several regions are defined spanwise, as highlighted by the different colors. Each region is assigned its own thickness and lamination parameters. The 3D mesh is significantly finer than the shell mesh to provide greater design freedom and enable the emergence of novel solutions.



(a) 3D mesh of the wingbox and strutbox core for topology optimization.



(b) Shell elements for composite optimization with the different zones.

Figure 9 – SBDW structural model mesh.

Regarding the strut-wing junction, the motion of all shell contour nodes at the end of the strut (green in Figure 10) is gathered around a reference node located at the middle of the profile (white point in Figure 10). Subsequently, a rigid connection links this reference node to distribute the load to all shell nodes of the wing (red in Figure 10), extending from the front end of the profile to the chord corresponding to the strut end.

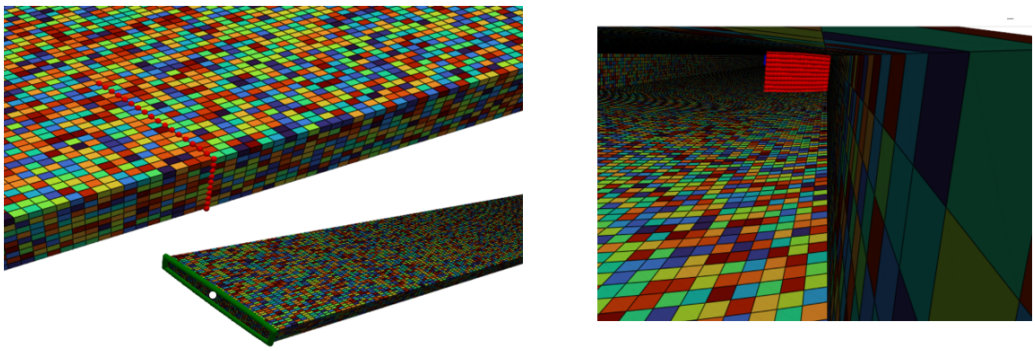


Figure 10 – 3D mesh detail for connection between the strut and the wing.

The discretized loads in the dry-wing configuration are introduced at the quarter chord, spaced out equally along the span. An illustration of the discretized lift distribution is displayed in Figure 11.

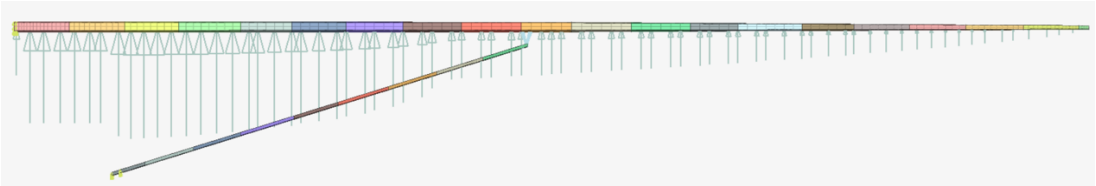


Figure 11 – Discretized loads for the 2.5 g MLA condition on the SBDW structural model.

4.1 Topology Optimization

4.1.1 Parametrization

The topology is parameterized by means of a density approach with an isotropic material. A scalar density value ρ is assigned to each 3D volumic element of the model. To obtain distinct solutions, the Solid Isotropic Material with Penalization (SIMP) interpolation [11] is used:

$$[Q] = \rho^p [Q_0], \tag{10}$$

in which $[Q_0]$ is the pristine stiffness tensor of the selected isotropic material, and $[Q]$ is the stiffness tensor used for mechanical analysis. The density ρ ranges between $[\rho_{\min}, 1]$, where $\rho_{\min}$ is set to 10^{-3} to avoid singularity problems with the FEM resolution. The aim of topology optimization is to find the optimized material distribution which consists mainly of absence ($\rho = \rho_{min}$) and presence ($\rho = 1$) of material. This is controlled through the SIMP penalization exponent p, taken as 3 herein. Furthermore, in order to have a length scale control and avoid numerical artifacts such as checkerboard, a filter is used [12].

The filtered densities are the physical variables which are used to compute the volume of the design space and to set up the FEM analysis with the stiffness tensor defined by Equation 10.

$$\widetilde{\rho}_i = \frac{\sum_{j \in \Omega_i} w_{ij} \rho_j}{\sum_{j \in \Omega_i} w_{ij}} \tag{11}$$

Ω_i is the set of elements whose centroids x_j are within the circle of radius R_ρ centered at the centroid x_i of element i. The associated filter weights w_{ij} are obtained as:

$$w_{ij} = R_\rho - |x_j - x_i| . \tag{12}$$

4.1.2 Strength Constraint

In the case of a strength criterion for topology optimization, stress singularities and numerical cost issues become an issue. Stress singularities arise when when ρ tends to $\rho_{\min}$, but the stress does not go towards 0. Therefore, low density elements are difficult to be removed from the design space. Several relaxation techniques are available to remediate this issue, of which the qp-approach [13] is used herein with q = 2.5. The relationship between stress $\{\sigma\}$ and strain $\{\varepsilon\}$ used to compute the value of the stress-based strength criterion then reads as:

$$\{\sigma\} = \rho^{p-q} [Q_0] \{\varepsilon\} , \tag{13}$$

The component of the stress tensor can then be used to computed the Von Mises stress σ^{VM} according to:

$$\sigma^{VM} = \sqrt{\frac{1}{2}\left[(\sigma_{11} - \sigma_{22})^2 + (\sigma_{22} - \sigma_{33})^2 + (\sigma_{33} - \sigma_{11})^2\right] + 3\left(\sigma_{12}^2 + \sigma_{23}^2 + \sigma_{31}^2\right)} . \tag{14}$$

A local material strength optimization constraint g can then be constructed at the element level, depending on σ^{VM} and the material yield stress σ^Y:

$$g := \frac{\sigma^{VM}}{\sigma^{Y}} \leq 0\,. \tag{15}$$

Finally, to avoid having many optimization constraints and a prohibitive numerical cost to compute the gradient of each local strength constraint, an P-norm aggregation function is used to approximate the maximum of all local strength constraint. This then becomes a single overall optimization constraint. In doing so, the gradient can be computed with an adjoint analysis. The aggregation is define on a subdomain Ω_k (with N_k elements) of the total model domain Ω. Introducing the aggregation parameter μ, the P-norm aggregation is then defined as:

$$g_k^{PN} := \left[\sum_{i\in\Omega_k} g_i^{\mu}\right]^{1/\mu}\,. \tag{16}$$

The optimization constraint associated with the elements in Ω_k is then $g_k^{PN} - 1 \leq 0$ [14].

4.2 Optimization Problem Statement

The structural optimization problem for topology and homogenized composite reads as:

$$\min_{\{\rho\},\{t\},\{V_A^1\},\{V_A^3\},\{V_D^1\},\{V_D^3\}} \text{mass}\,(\{\rho\},\{t\})$$
$$\text{s.t.} \begin{cases} \text{strength}(\{\rho\},\{t\},\{V_A^1\},\{V_A^3\},\{V_D^1\},\{V_D^3\}) \\ C(\{\rho\},\{t\},\{V_A^1\},\{V_A^3\},\{V_D^1\},\{V_D^3\}) \leq C_0 \\ (1-4p)^2 + (1-4p)\{V_A^3\} - 2\{V_A^1\}^2 \geq 0 \\ 1-4p-\{V_A^3\} \geq 0 \\ 1+\{V_D^3\} - 2\{V_D^1\}^2 \geq 0 \\ 1-\{V_D^3\} \geq 0 \\ \{t\} \in [t_{\min}, t_{\max}] \\ \{V_{A,D}^{1,3}\} \in [-1,1] \\ \{\rho\} \in [\rho_{\min}, 1] \end{cases} \tag{17}$$

The topology optimization part is performed with an isotropic material and properties, whereas the composite optimization is performed with a homogenized approach as described in Section 3.1. The methodology still considers elastic materials within the assumptions of small strains and small displacements, the mechanical response is obtained from a mechanical analysis by means of the FEM.

The homogenized composite contribution is characterized by the thickness and LP design variables of the shell elements that represent the surface (skin and spar) of the wingbox and strutbox. The topology optimization is represented by the density variable $\{\rho\}$, assigned to each 3D elements. Both the homogenized composite and topology have an influence on the mechanical responses.

The objective of the optimization is still to minimize the mass of the structure under several load cases. However, the constraints now are the compliance and strength. Compliance C is the inverse of the structure stiffness, and is obtained as $C = \{U\}^T[K]\{U\}$. It should be lower than the target compliance C_0. The target compliance is obtained as the results of the optimization of Equation 7 for the same load cases. The strength constraints consists of both the strength in the composite part according to Equation 6, and according to Equation 16 for the isotropic topology optimization part. For the latter, only one cluster is considered for the aggregation of the topology optimization strength, containing all 3D elements. The optimization problem is still solved using the gradient-based optimization algorithm SQP, all within Optistruct [8].

5. Results

5.1 Conventional Wing Configuration

5.1.1 Homogenized Composite Optimization

The first-step homogenized composite optimization has been carried out on the SBW, and compared to a *black aluminum* optimization. Five gradient-optimization of Problem 7 are done for up to 50 iterations each with an update of the loads in between to consider the change in wing mass due to the optimization.

The mass distribution for the different components is shown in Figure 12 for both optimizations. The mass proportion of the components in both optimizations is similar, with the composite results being much lighter thanks to the additional design freedom of the layups, but also the larger tensile range of the allowables. The result of the composite optimization, with the LP distribution, is shown in Figure 15.

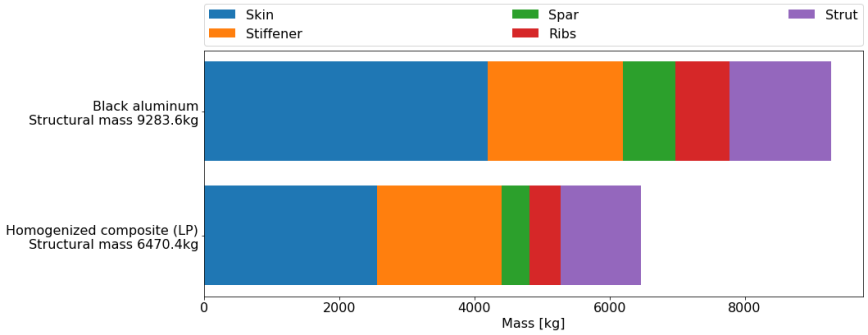


Figure 12 – Mass distribution of two optimized SBW, for a *black aluminum isotropic* material and homogenized composite optimization.

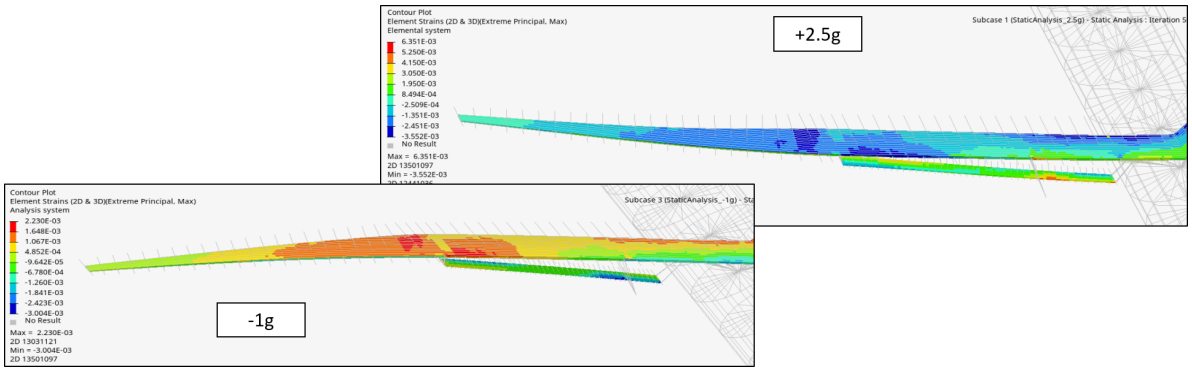


Figure 13 – Principal strain distribution of the first level optimization of the conventional design.

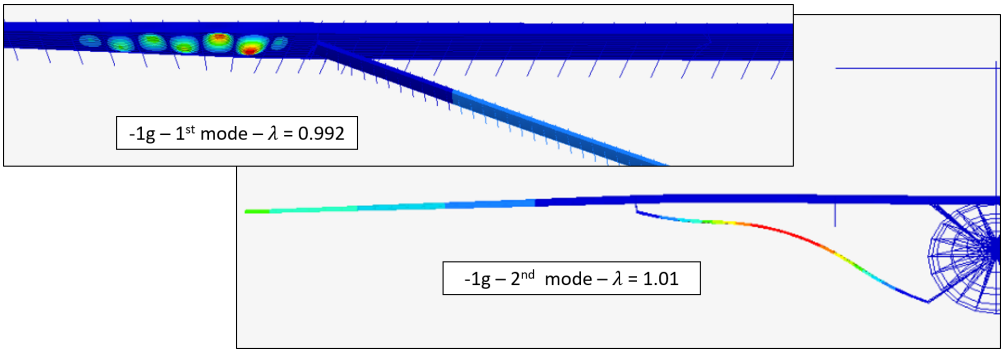


Figure 14 – Linear buckling modes of the first level optimization of the conventional design.

The mechanical response, in terms of strain distribution and buckling modes, is shown in Figures 13 and 14, respectively. The strain distribution reveals a subtle influence of the relative strut–wing sweep [4], manifested through the in-plane bending moment acting on the inboard wing section between the strut attachment and the fuselage. As a result, the strength constraint is not uniform along the chord but varies in both the chordwise and spanwise directions. Regarding buckling, the first few modes become nearly coalescent by the end of the optimization. The second mode corresponds to a characteristic strut-braced wing (SBW) buckling pattern, involving strut instability under negative load cases when the strut is subjected to compressive loading.

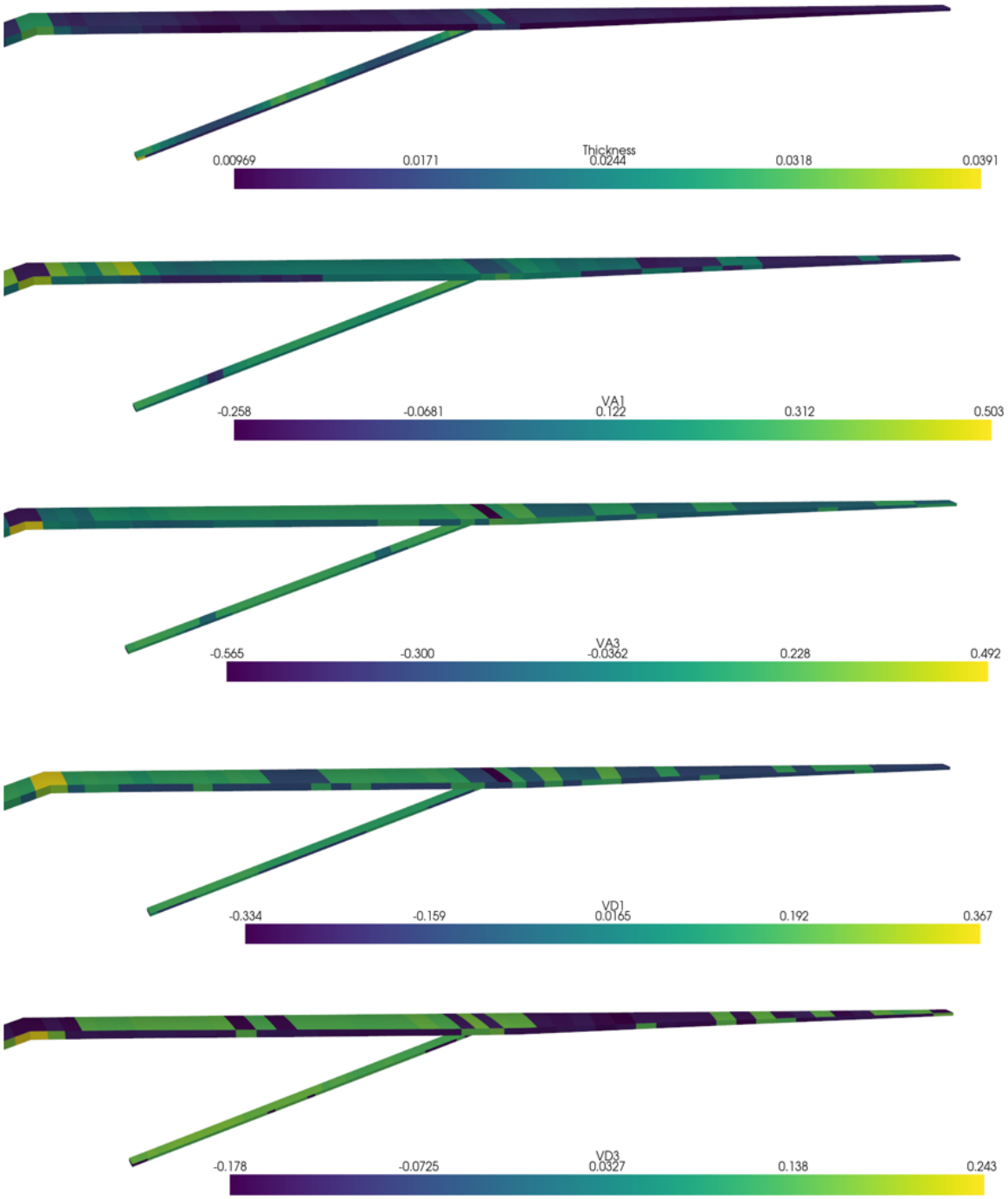


Figure 15 – Thickness and homogenized composite stiffness distribution of the conventional design.

5.1.2 SST Fiber Retrieval

From the first level homogenized results, a SST is retrieved. This process is carried out independently for the wingbox and the strutbox, as these structural components are connected through dedicated mechanical connectors, eliminating the requirement for ply continuity at the wing–strut junction. Steered fibers are considered, with an equivalent steering radius between 2 zones of 2.5 m. The optimization of Equation 8 is performed 3 times for each SST, with each 2000 iterations of the genetic algorithm. Each iteration has 100 individuals, while the 25 best individuals are kept for the archive. The best solution is the SST with the lowest objective (= stiffness difference) of the 3 runs. The convergence of the SST optimization of the wingbox SST is shown in Figure 16.

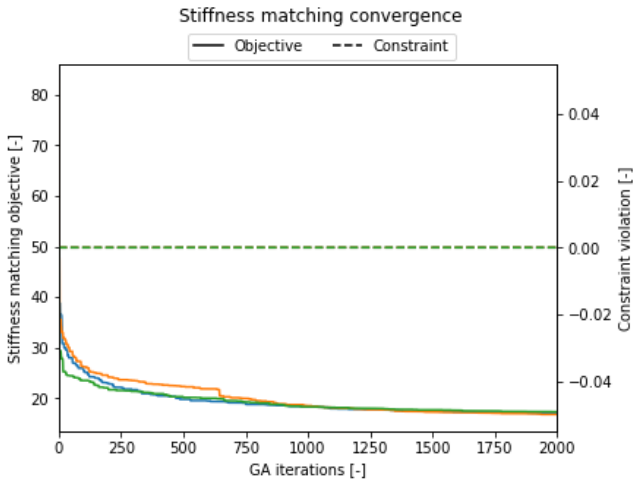
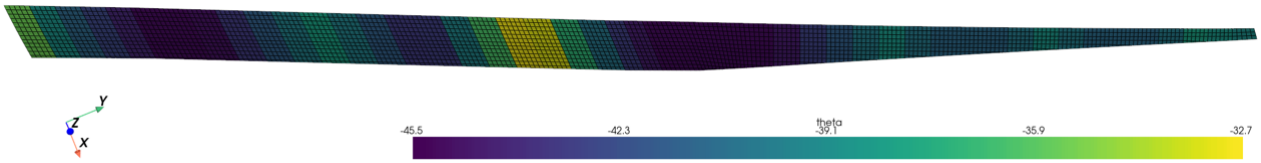
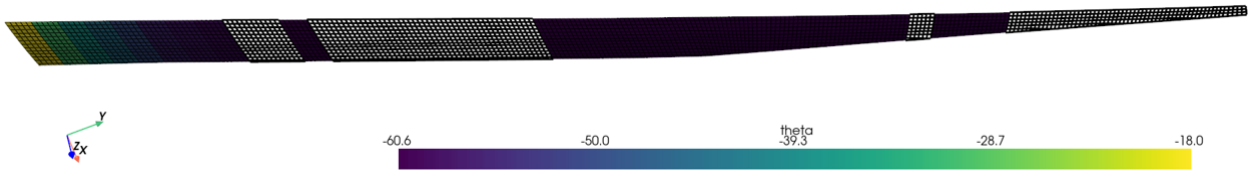


Figure 16 – Convergence graph of the 3 *stiffness matching* optimizations with steered fiber for the SBW.

The ply number varies between 15 and 220, only a few are shown here as a visualization representation. Two plies of the top skin are displayed in Figure 17. Figure 17a shows a continuous ply that covers the complete wing and is present in each zone, where the fiber steering over the span is well visible. The equivalent steering radius dictates the rate of variation of the orientations between adjacent zones, with this radius going to infinite only straight fibers are obtained. Figure 17b on the other hand shows patches of ply for certain zones, as it is only present in the thicker laminates.



(a) Steered ply covering the complete top skin.



(b) Steered ply covering part of the top skin, present for thicker laminates.

Figure 17 – Ply for the top skin of the SBW.

Finally, a representation of the *stiffness matching* is presented in Figure 18. For the different considered ply thicknesses (represented by a horizontal slice), the figure compares the lamination parame-

ter (LP) values associated with the in-plane stiffness matrix (V_A^1 and V_A^3) and the bending stiffness matrix (V_D^1 and V_D^3) obtained from the first-level optimization with those resulting from the different layups generated through the SST. The results show that the first-level LP values are more dispersed, as they are treated as independent design variables during the optimization. In contrast, the LP values associated with the SST solutions are significantly more clustered. This behavior is expected, since the SST-derived LP variations are constrained by the requirement of a continuous manufacturable layup, which cannot be modified independently at will.

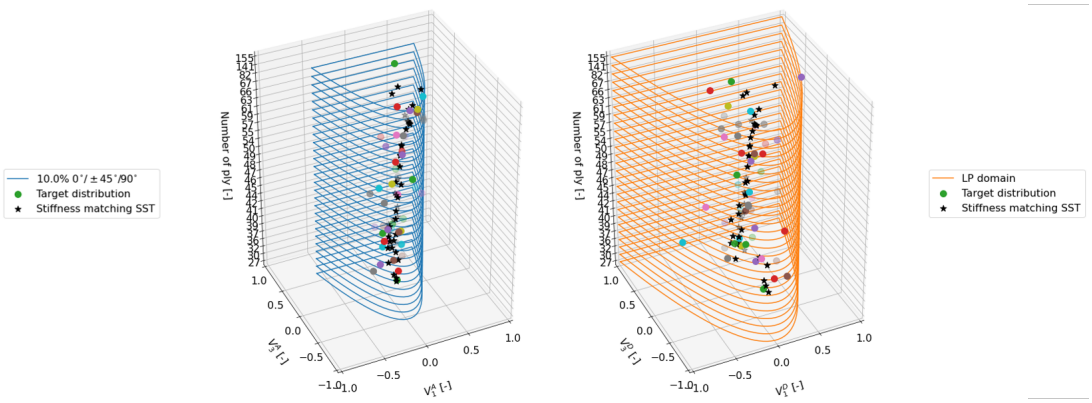


Figure 18 – SST homogenized stiffness distribution compared to the first level stiffness distribution. A different SST is used for the wingbox and strutbox.

5.2 Dry-Wing Concept

5.2.1 Topology and Homogenized Composite Optimization

The combined topology and homogenized composite optimization is performed for a fixed 200 iterations, limited by the numerical cost of the optimization. A filter of 0.1 m is used for the topology optimization part. The convergence graph of the optimization is displayed in Figure 19. It shows that for the first few iterations the mass barely changes, while the worst constraint decreases. Once all constraints are satisfied, the optimization starts minimizing the mass. During later iterations, some constraints become violated again, but this does not hinder the convergence, as these violations are subsequently resolved and constraint satisfaction is restored.

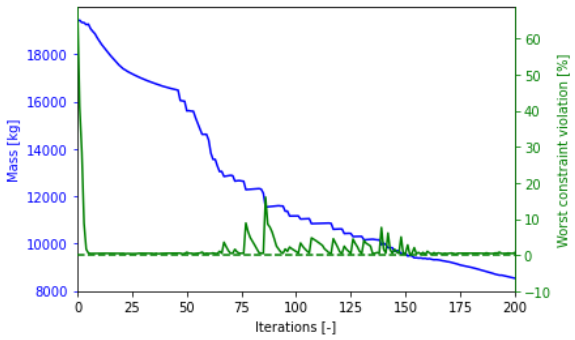


Figure 19 – Convergence of the combine topology and homogenized composite optimization of a SBDW.

The distribution of the homogenized composite properties is displayed in Figure 20. The thickness profile distribution shows a peak of thickness at the root and strut-wing junction, to satisfy the strength constraint where high local internal loads are transferred between the strut and wing. Furthermore, the homogenized composite initialization starts from a Quasi-Isotropic (QI) layup, meaning all 4 LPs $V_{A,D}^{1,3} = 0$, with the optimization obtaining rather constant but different from QI properties, with some

variation at the location of varying thickness.

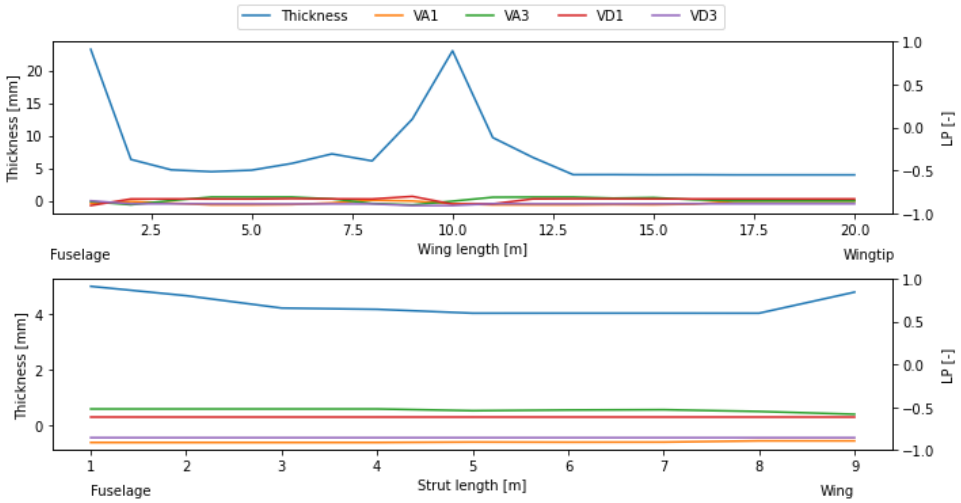


Figure 20 – Convergence of the combined topology and homogenized composite optimization of a SBDW: wing properties on the top, and strut properties on the bottom.

Finally, Figure 21 displays the topology optimization results. The wing core concentrates most of the material towards the strut junction to prevent strength constraint violations arising from the transfer of strut forces into the wing. In contrast, minimal core material is present towards the wingtip. Conversely, the inboard section present a specific pattern, having more material towards the top of the leading edge and the bottom of the trailing edge. Indeed, the core material is arranged to stiffen the region against in-plane bending moments, ensuring that the compliance constraints are met. Concerning the strut, its core remaining largely solid to function as an axial rod, thereby enhancing the system stiffness.

Notably, no buckling constraint was included in this optimization. Although skin buckling is typically a primary driver for the use of ribs and stiffeners, its exclusion is due to the current complexity of integrating buckling constraints into composite topology optimization, a topic that remains an open challenge in academic research. Consequently, the absence of core material and the resulting emergence of novel load paths are directly linked to this missing buckling constraint. Addressing this limitation should be the next step to improve the fidelity of the SBDW structural design.

https://doi.org/10.71945/icas2026_0355

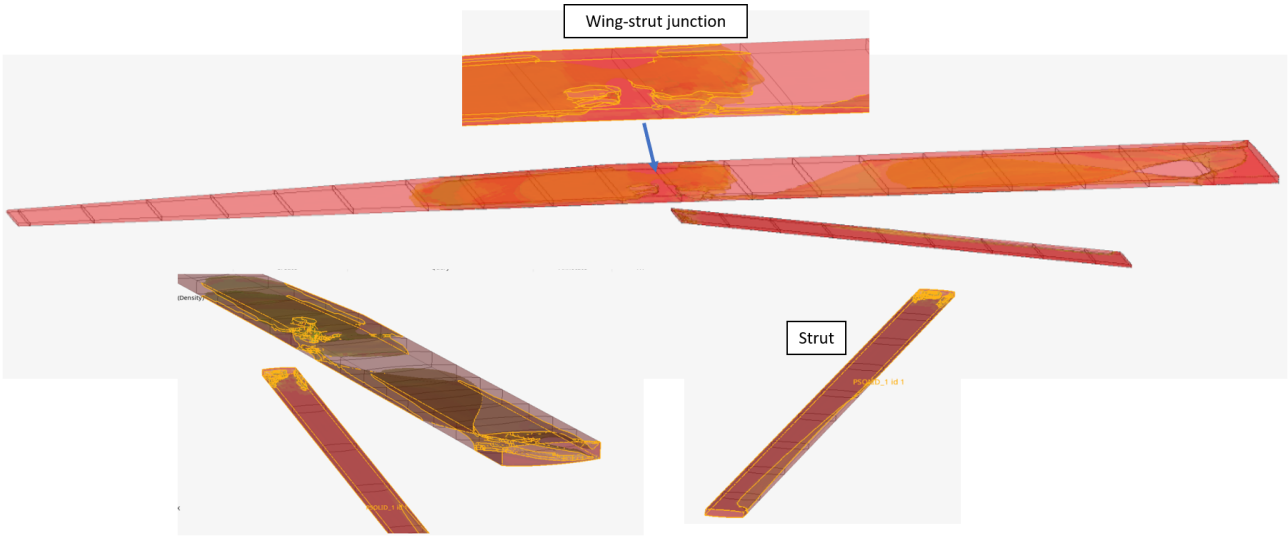


Figure 21 – Topology optimization result of the core of the wing and strut, with elements shown for $\rho \geq 0.9$.

5.2.2 SST Fiber Retrieval

A fiber retrieval is performed by means of *stiffness matching* of Equation 8 with respect to the homogenized results. Two independent SST are optimized, one for the wing and another one for the strut. The same optimization settings as in Section 5.1.2 are used, with an equivalent fiber steering radius of 2.5 m.

Focus is placed on the strut, as the reduced ply count helps visualize the complete layup results. The actual layup of each strut zone from the optimized SST is displayed in Table 4. The orange, gray and purple cells are continuous plies for the complete strut, whereas the green and blue are plies that are inserted for the higher thickness zones only. The overall ply drop, and subsequent thickness profile of the layup matches closely the thickness line distribution for the strut that was presented in the bottom graph of Figure 20. The third continuous ply from the top layer is represented in Figure 22.

A physical symmetric and balanced layup can only be ensured when the number of plies is a multiple of four; for any other ply count, either the physical symmetric or balanced conditions will inevitably be violated. This limitation is inherent to laminate design. However, the impact of unsymmetry and unbalance is mitigated through the stiffness matching objective. In the first-level optimization, all layups are enforced to remain symmetric and balanced ($V_{2,4}^{A,D} = 0$ by definition of the optimization problem). Consequently, the objective is to minimize the unbalance (shear-axial coupling) and unsymmetrical (axial-bending) coupling.

This is only half the actual layup, as it is symmetric about the midplane. For zones with an odd number of plies, the symmetry is not conserved and one ply is dropped on the mirrored half of the layup. Furthermore, the balanced rule is well visible, as for any $+\theta$ steered ply, an opposite $-\theta$ steered ply can be found in the layup, except again for odd plies. A similar layup is obtained from the optimized SST for the wing.

Table 4 – Half actual layup of the different strut zones, with the ply colors showing continuous plies for the insertion value of 0.

	Fuselage side							Wing side		
Zone	1	2	3	4	5	6	7	8	9	X_{ins}
X_{ply} [-]	24	22	22	21	21	21	22	25	26	
Bottom layer	32.6							33.6	31.8	0
	-15.0	34.3	35.6				34.3	-15.0	-15.0	0
	-32.6	-15.2	-15.4	35.9	35.8	35.3	-15.0	-33.6	-31.8	0
	51.9	-34.3	-35.6	-15.2	-15.0	-15.0	-34.3	46.9	50.0	0
	-51.9	56.1	59.6	-35.9	-35.8	-35.3	48.9	-46.9	-50.0	0
	15.0	-56.1	-59.6	59.6	56.7	52.6	-48.9	15.0	15.0	0
	-87.5	15.2	15.4	-59.6	-56.7	-52.6	15.0	-84.3	-86.6	1
	-87.6	-88.9	-89.3	15.2	15.0	15.0	-85.1	-84.8	-87.1	0
	87.6	-88.3	-88.6	-88.2	-87.3	-86.2	-85.3	84.8	87.1	0
	87.5	88.3	88.6	88.2	87.3	86.2	85.3	84.3	86.6	3
	89.7	89.9	90.0	90.0	90.0	90.0	89.8	89.7	89.5	0
Symmetry plane	-89.7	-89.9	-90.0	-90.0	-90.0	-90.0	-89.8	-89.7	-89.5	0

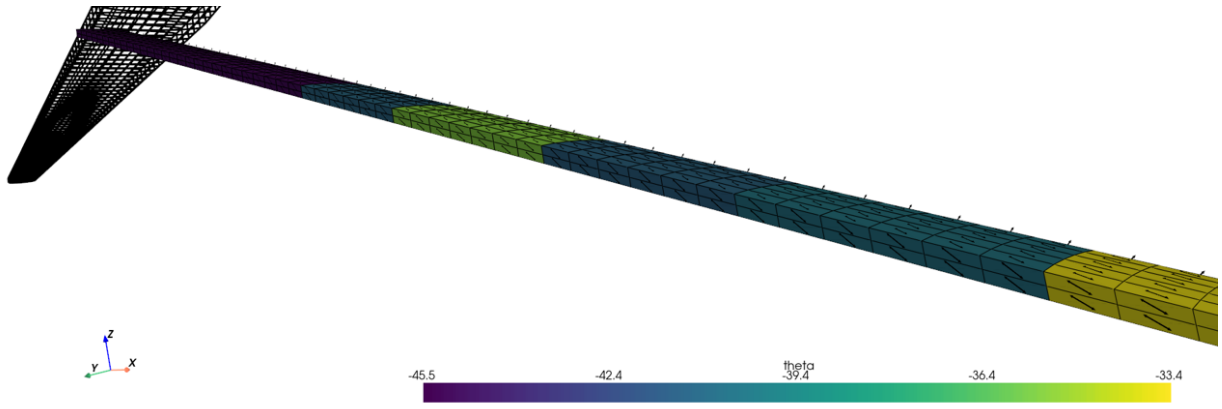


Figure 22 – Full steered ply of the strut SST.

6. Conclusions

This paper presents the methodology and results of the advanced structural optimization of a Strut-Braced Wing (SBW) on a fixed aircraft configuration. The configuration is the best outcome of a multidisciplinary optimization of a hydrogen concept within the Clean Aviation UP Wing project. The structural design of the SBW is based on the composite optimization of a conventional wingbox and strutbox concept with ribs and stiffeners for a mass minimization under strength and buckling constraints. The three considered loadcases are a ± 1 g elliptical lift distribution, and a 2.5 g Maneuver Load Alleviation (MLA) that reduces the wing tip loading. The composite optimization is performed in a bi-level framework. First, balanced and symmetrical laminate stiffness is defined by 4 Lamination Parameters (LP). Along with a continuous thickness variable, they constitute the design variables for the structural optimization. The optimized composite wing is lighter than the equivalent isotropic design for the same structural problem. This is partly due to higher strength allowables, but also to the increased design freedom enabled by stiffness tailoring for a fixed thickness. Afterwards, a second step aims at retrieving the actual layup based on *stiffness matching* of the discrete layups to match the required first level homogenized stiffness. To obtain continuous plies for the wing, a Stacking Sequence Table (SST) concept is used, applied to steered fibers.

The concept of an innovate Strut-Braced Dry Wing is considered afterwards, where in the internal volume the ribs and stiffeners within the internal volume are replaced by a 3D mesh that fills the core of both the wingbox and strutbox. The mesh is used to perform topology optimization to assess

possible new internal load bearing structures, while a bi-level composite optimization is still applied on the spars and skins. The structural optimization is performed for the same load cases, with a strength constraint but considering a compliance constraint instead of buckling. The results highlight that, for the considered SBDW optimization without accounting for buckling, the load path associated with stiffness maximization in the wing leads to the removal of most of the core material, while material is predominantly retained in the strut. In the wing core, material remains primarily at the strut and fuselage junctions in order to redistribute the locally high load introduction. Further development of the dry wing configuration using topology optimization should also incorporate buckling constraints. Finally, a *stiffness matching* fiber retrieval step is again performed, which illustrated expected outputs in the form of the different layups and ply continuity across different zones with fiber steering by using a SST.

7. Contact Author Email Address

lander.vertonghen@onera.fr; charly.mollet@onera.fr; cedric.julien@onera.fr; francois-xavier.irsarri@onera.fr

8. Grant agreement

The project Ultra Performance Wing (UP Wing, project number: 101101974) and ACAP (project number: 101101955) are supported by the Clean Aviation Joint Undertaking and its members. DISCLAIMER: Co-Funded by the European Union. Views and opinions expressed are however those of the author(s) only and do not necessarily reflect those of the European Union or Clean Aviation Joint Undertaking. Neither the European Union nor the granting authority can be held responsible for them.

9. Copyright Statement

The authors confirm that they, and/or their company or organization, hold copyright on all of the original material included in this paper. The authors also confirm that they have obtained permission, from the copyright holder of any third party material included in this paper, to publish it as part of their paper. The authors confirm that they give permission, or have obtained permission from the copyright holder of this paper, for the publication and distribution of this paper as part of the ICAS proceedings or as individual off-prints from the proceedings.

References

[1] Michaël Méheut, Diego Losada Costoso, Frédéric Moëns, Olivier Atinault, Cédric Julien, Lander Vertonghen, Ludovic Coelho, Valentin Priasso, Antoine Lannoo, Sébastien Defoort, Eric Nguyen Van, Christophe David, Dimitrios Glenis, J. Sodja, S. de Boer, J. Schwingel, and D. Eisenhut. Strut-Braced Dry Wing Concept for Hydrogen-Powered Aircraft. In *34th Congress of the International Council of the Aeronautical Sciences (ICAS 2024)*, Florence, Italy, September 2024.

[2] Enrico Stragiotti, Eric Nguyen Van, Sébastien Defoort, Michaël Méheut, Olivier Atinault, Diego Losada Costoso, Charly Mollet, Frédéric Moëns, Cédric Julien, Lander Vertonghen, Valentin Priasso, and Antoine Lannoo. SWIFT: a ultra high aspect ratio strut-braced dry wing hydrogen-powered aircraft. In *35th Congress of the International Council of the Aeronautical Sciences (ICAS 2026)*, Sidney, Australia, September 2026. International Council of the Aeronautical Sciences.

[3] Diego Losada Costoso, Olivier Atinault, Michaël Méheut, Guillaume Starck, Enrico Stragiotti, and Eric Nguyen Van. Aerodynamic Transonic Design of a Strut-Braced Wing. In *35th Congress of the International Council of the Aeronautical Sciences (ICAS 2026)*, Sidney, Australia, September 2026. International Council of the Aeronautical Sciences.

[4] Charly Mollet, Lander Vertonghen, and Cédric Julien. Aeroelastic design of a strut-braced dry wing for a hydrogen aircraft in an MDO framework. In *35th Congress of the International Council of the Aeronautical Sciences (ICAS 2026)*, Sidney, Australia, September 2026. International Council of the Aeronautical Sciences.

[5] Stephen W. Tsai and Thomas H. Hahn. *Introduction to Composite Materials*. Technomic Publishing Company, Lancaster, 1980.

[6] Stephen W. Tsai and NIcholas H. Pagano. Invariant properties of composite materials. Technical report, 1968.

[7] Mostafa Abdalla, Zafer Gurdal, and Christos Kassapoglu. Formulation of Composite Laminate Robustness Constraint in Lamination Parameters Space. In *50th AIAA/ASME/ASCE/AHS/ASC Structures, Structural Dynamics, and Materials Conference*, Structures, Structural Dynamics, and Materials and Co-located Conferences. American Institute of Aeronautics and Astronautics, May 2009.

[8] Altair Engineering Inc. *Altair OptiStruct, Version 2025*. Troy, Michigan, USA, 2025. `https://altair.com/optistruct`.

[9] F.-X. Irisarri, A. Lasseigne, F.-H. Leroy, and R. Le Riche. Optimal design of laminated composite structures with ply drops using stacking sequence tables. *Composite Structures*, 107:559–569, January 2014.

[10] Lander Vertonghen, Cédric Julien, Attilio Chiappini, and François-Xavier Irisarri. Introducing fiber steering in a stacking sequence table for improved performance matching in a bi-level composite optimization. In *22th European Conference on Composite Materials*, Oslo, Norway, June 2026.

[11] Martin P. Bendsøe and Ole Sigmund. *Topology Optimization*. Springer Berlin Heidelberg, Berlin, Heidelberg, 2004.

[12] O. Sigmund and J. Petersson. Numerical instabilities in topology optimization: A survey on procedures dealing with checkerboards, mesh-dependencies and local minima. *Structural optimization*, 16(1):68–75, August 1998.

[13] Matteo Bruggi. On an alternative approach to stress constraints relaxation in topology optimization. *Structural and Multidisciplinary Optimization*, 36(2):125–141, August 2008.

[14] Chau Le, Julian Norato, Tyler Bruns, Christopher Ha, and Daniel Tortorelli. Stress-based topology optimization for continua. *Structural and Multidisciplinary Optimization*, 41(4):605–620, April 2010.